

Probing inhomogeneous cuprate superconductivity by terahertz Josephson echo spectroscopy

Received: 29 October 2023

Accepted: 16 August 2024

Published online: 16 September 2024

 Check for updates

A. Liu^{1,2}✉, D. Pavićević¹, M. H. Michael¹, A. G. Salvador³, P. E. Dolgirev⁴, M. Fechner¹, A. S. Disa^{1,5}, P. M. Lozano^{2,6}, Q. Li^{2,6}, G. D. Gu², E. Demler³ & A. Cavalleri^{1,7}✉

Inhomogeneities crucially influence the properties of quantum materials, yet methods that can measure them remain limited and can access only a fraction of relevant observables. For example, local probes such as scanning tunnelling microscopy have documented that the electronic properties of cuprate superconductors are inhomogeneous over nanometre length scales. However, complementary techniques that can resolve higher-order correlations are needed to elucidate the nature of these inhomogeneities. Furthermore, local tunnelling probes are often effective only far below the critical temperature. Here we develop a two-dimensional terahertz spectroscopy method to measure Josephson plasmon echoes from an interlayer superconducting tunnelling resonance in a near-optimally doped cuprate. The technique allows us to study the multidimensional optical response of the interlayer Josephson coupling in the material and disentangle intrinsic lifetime broadening from extrinsic inhomogeneous broadening for interlayer superconducting tunnelling. We find that inhomogeneous broadening persists up to a substantial fraction of the critical temperature, above which this is overcome by the thermally increased lifetime broadening.

Unconventional superconductivity in cuprates emerges when either electrons or holes are doped into the insulating parent compound. Because superconductivity is optimized far away from optimal stoichiometric composition, disorder of the host lattice is unavoidable and may result in substantial electronic inhomogeneities^{1,2}. Measurements of the electronic properties of cuprates using scanning tunnelling microscopy³ reveal disorder of the superconducting gap on nanometre length scales^{4,5}, whose variations are further correlated with the distribution of dopant atoms⁶. Yet the potential presence of co-existing and competing orders complicates the assignment of observables to superconductivity. Modern techniques based on

tunnelling from a superconducting tip⁷ can now isolate the superconducting response^{8–11} but are still limited to sampling surfaces amenable to tip-based techniques and temperatures typically below that of liquid helium. Additional probes of the role of these inhomogeneities on the superconducting order parameter are therefore necessary to obtain a complete picture of the role of disorder in these materials.

The tunnelling resonance arising from Josephson coupling between adjacent superconducting CuO₂ planes, the so-called Josephson plasma resonance^{12,13}, provides a direct measure of the superconducting order parameter and of the *c*-axis transport^{14,15}. The Josephson

¹Max Planck Institute for the Structure and Dynamics of Matter, Hamburg, Germany. ²Condensed Matter Physics and Materials Science Division, Brookhaven National Laboratory, Upton, NY, USA. ³Institute for Theoretical Physics, ETH Zurich, Zurich, Switzerland. ⁴Department of Physics, Harvard University, Cambridge, MA, USA. ⁵School of Engineering and Applied Physics, Cornell University, Ithaca, NY, USA. ⁶Department of Physics and Astronomy, Stony Brook University, Stony Brook, NY, USA. ⁷Department of Physics, University of Oxford, Oxford, UK. ✉e-mail: aliu1@bnl.gov; andrea.cavalleri@mpsd.mpg.de

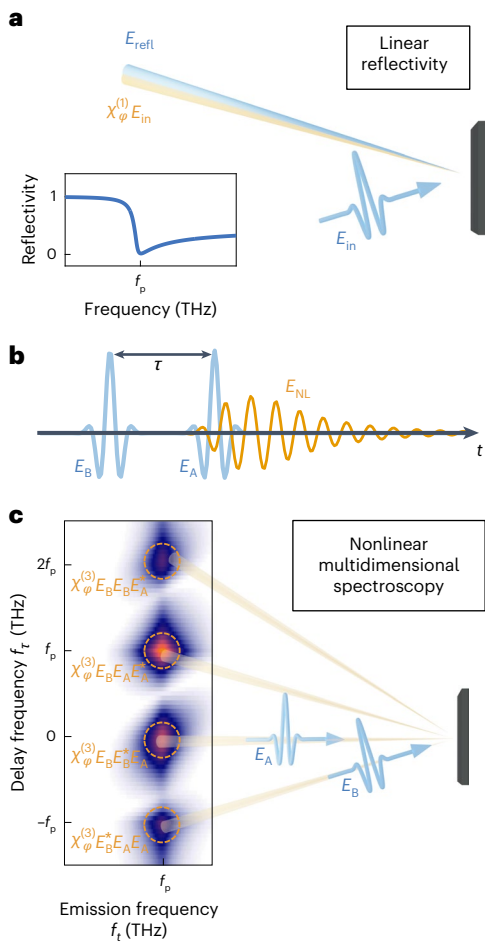


Fig. 1 | Linear and nonlinear spectroscopies of plasma resonances.

a, A schematic of a linear reflectivity measurement, in which an incident field E_{in} induces a linear response $\chi_{\varphi}^{(1)}$. The co-propagating reflected field E_{refl} and the linear response $\chi_{\varphi}^{(1)}$ interfere to produce a characteristic edge in the reflectivity shown (inset). **b**, The generation of a nonlinear electric field E_{NL} by two excitation pulses E_A and E_B of comparable amplitude. The amplitude and phase of E_{NL} depend on the inter-pulse time delay τ . **c**, A schematic of nonlinear multidimensional spectroscopy, in which Fourier transform of E_{NL} along the two time variables $\{\tau, t\}$ resolves a nonlinear optical response $\chi_{\varphi}^{(3)}$ in a 2D spectrum. In the non-collinear excitation geometry shown, various components of $\chi_{\varphi}^{(3)}$ are emitted in unique phase-matched directions shown.

plasma resonance has been extensively studied by linear spectroscopy, in which the c -axis reflectivity exhibits a pronounced plasma edge in the superconducting state (Fig. 1a). Van der Marel and Tsvetkov first pointed out¹⁶ that a distribution of Josephson plasma frequencies, reflecting disorder of the superconducting order parameter, manifests as a distortion of the Josephson plasmon loss function¹⁷. Corresponding distortion of the reflectivity edge profile was then exploited by Dordevic et al.¹⁸ to quantify the underlying disorder in $\text{La}_{2-x}\text{Sr}_x\text{CuO}_4$.

However, this approach suffers from various shortcomings. For example, in ref. 18, the lineshape fits based on a two-fluid model are generally not completely constrained and require assumptions on both the normal fluid conductivity and the functional form of the plasma frequency distribution. Reliable fits are also only possible at low temperatures, in which a sharp plasma edge is observed.

To circumvent these limitations, techniques capable of resolving higher-order plasmon correlation functions are required. These higher-order plasmon correlations may be measured by nonlinear spectroscopy^{19,20}, an example of which is shown schematically in Fig. 1b where two excitation fields E_A and E_B cooperatively generate a nonlinear

electric field E_{NL} . The depicted nonlinear process is governed by a third-order optical response $\chi_{\varphi}^{(3)}$, with multiple frequency and wavevector components. These may be resolved in a two-dimensional (2D) spectrum^{21,22} (Fig. 1c) by Fourier transforming E_{NL} along the inter-pulse time delay τ and the emission time t . So-called 2D spectroscopy has been implemented at terahertz frequencies in collinear excitation geometries to study a variety of material systems^{23–35}, including superconductors more recently^{36–38}.

Previous applications of 2D terahertz spectroscopy have all implemented a collinear geometry, in which the excitation fields and nonlinear signal emission all possess identical wavevectors. While convenient, such a collinear geometry cannot isolate specific nonlinearities and further precludes study of opaque materials. We therefore implement a non-collinear excitation geometry with which different components of $\chi_{\varphi}^{(3)}$, corresponding to different peaks in the 2D spectrum, are emitted in unique phase-matched directions (Fig. 1c).

The non-collinear phase-matching geometry is shown in Fig. 2a, in which two quantities are conserved. In addition to the momentum magnitude determined by the Josephson plasma frequency, only in-plane momentum is conserved due to the interface³⁹. For fixed excitation and detection geometry, the nonlinearity arriving at the detector may be chosen by rotating the sample and thereby the in-plane momentum of each excitation beam (Fig. 2b).

We demonstrate this principle in Fig. 2c on near-optimally doped $\text{La}_{2-x}\text{Sr}_x\text{CuO}_4$ ($x = 0.17$, LSCO), which exhibits a Josephson plasma resonance with resonance frequency $f_p \approx 2$ THz at temperatures far below the phase transition ($T \ll T_c$). All four components of $\chi_{\varphi}^{(3)}$ that radiate at the Josephson plasma frequency^{40,41} are resolved at their respective phase-matching conditions (described in Supplementary Section 2). In contrast to linear spectra, which exhibit broad features due to the presence of both normal and superconducting optical responses, the optical nonlinearities of superconducting carriers are orders of magnitude stronger than those of the normal carriers, resulting in sharp peaks that reflect solely the superconducting response. Here, we focus on the nonlinearity appearing at $(f_e, f_t) = (2, -2)$ THz, which corresponds to a terahertz frequency ‘Josephson echo’.

The advantage of Josephson echoes in measuring disorder is illustrated by Fig. 3, in which two cartoons of homogeneous and disordered interlayer tunnelling are shown in Fig. 3a. If intrinsic spectral broadening of the resonance (for example, due to quasiparticle screening) is comparable to a distribution of Josephson plasma frequencies (due to variations in the interlayer tunnelling response), comparable optical responses are observed by linear optical spectroscopy (simulated comparisons between homogeneous and disordered spectra for reflectivity, loss function and optical conductivity are presented in Supplementary Section 6) and it is difficult to distinguish between these two physically distinct situations as shown in Fig. 3b.

This ambiguity is eliminated in a 2D spectrum, specifically in the spectral lineshape of the Josephson echo peak⁴². In the case of a homogeneous Josephson plasma resonance, the peak is symmetric with identical peak widths along the two frequency axes. In the presence of disorder, however, the Josephson echo peak develops a marked asymmetry from projecting disorder line-broadening into an orthogonal direction from the intrinsic linewidth of the resonance. We emphasize that the Josephson echo peak is the only nonlinearity that separates intrinsic and extrinsic broadening mechanisms, which may be understood by referring to its frequency coordinates that are opposite in sign. Microscopically, this reflects an effective time-reversal operation induced by the second excitation pulse that cancels extrinsic dephasing due to disorder (that is, from a distribution of Josephson plasma frequencies).

Measured 2D spectra of the Josephson echo in LSCO are shown in Fig. 4 for increasing temperatures approaching $T_c \approx 36$ K. At the lowest measured temperature of 6 K, the Josephson echo peak is asymmetric with a characteristic ‘almond’ shape that reveals a finite degree of

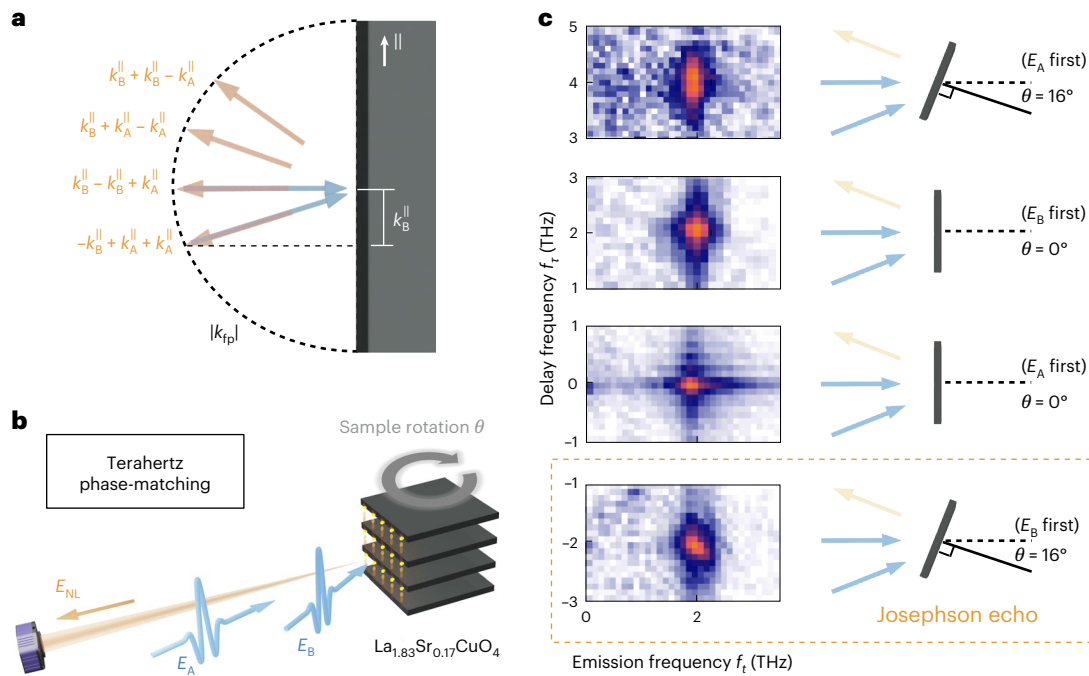


Fig. 2 | Phase-matching resolves individual plasmon nonlinearities. **a**, A schematic of wavevector phase-matching, in which momentum is only conserved along the in-plane (\parallel) direction and in its magnitude $|k_{\text{fp}}^{\parallel}|$. **b**, Sample rotation changes the in-plane momenta of each excitation field and determines the nonlinearity that arrives at the detector. **c**, Experimental measurements of the constituent components of $\chi_{\varphi}^{(3)}$ in $\text{La}_{1.83}\text{Sr}_{0.17}\text{CuO}_4$ are shown with the

corresponding sample rotation angles. The $(f_r, f_t) = (2, \pm 2)$ THz peaks are measured with E_B arriving first, followed by E_A . The $(2, 0)$ and $(2, 4)$ THz peaks are measured with E_A arriving first, followed by E_B . The $(2, -2)$ THz peak corresponds to an emitted Josephson echo. The full phase-matching conditions for both time orderings are described in Supplementary Section 2.

disorder^{42,43}. At higher temperatures, the peak becomes increasingly symmetric, suggesting a crossover into the regime of dominant intrinsic line-broadening. Next, we quantify this statement by extracting the individual intrinsic and disorder contributions to the Josephson plasma resonance peak width.

In 2D spectra, the disorder linewidth γ_{disorder} is projected into a characteristic direction along the ‘diagonal’ ($|f_t| = |f_r|$) line, in contrast to the intrinsic linewidth $\gamma_{\text{intrinsic}}$ that results in symmetric broadening. One may intuitively understand this behaviour by interpreting the vertical and horizontal frequency axes as the frequencies of initial terahertz absorption and final terahertz emission respectively, causing each excitation in the continuum of Josephson couplings to appear at a unique position along the diagonal. In the limit of dominant disorder ($\gamma_{\text{disorder}} \gg \gamma_{\text{intrinsic}}$), the lineshapes along the ‘diagonal’ and perpendicular ‘anti-diagonal’ directions are decoupled^{42,44} and depend solely on γ_{disorder} and $\gamma_{\text{intrinsic}}$, respectively⁴². In the present case of comparable intrinsic and disorder broadening, however, the two lineshapes must be simultaneously fit⁴³ to extract γ_{disorder} and $\gamma_{\text{intrinsic}}$.

Slices of the Josephson echo peak at 6 K are plotted in Fig. 5a, along the directions shown in the insets. The lineshape along the ‘diagonal’ direction (orange) is broader than the lineshape along the ‘anti-diagonal’ direction (blue), and the difference between the two peak widths indicates disorder line-broadening. Simultaneous fits of the two lineshapes (to phenomenological functional forms described and justified in Supplementary Section 3) were performed, from which we extract values of $\gamma_{\text{disorder}} = 0.08$ THz and $\gamma_{\text{intrinsic}} = 0.38$ THz. This value for γ_{disorder} is comparable to that reported by Dordevic et al.¹⁸ from linear reflectivity, which was extracted under an assumed value for $\gamma_{\text{intrinsic}}$.

In the linear optical response, the reflectivity edge associated with superconductivity rapidly fades into a featureless background with increasing temperature¹⁴. However, 2D terahertz spectroscopy distils the superfluid response from this normal fluid background

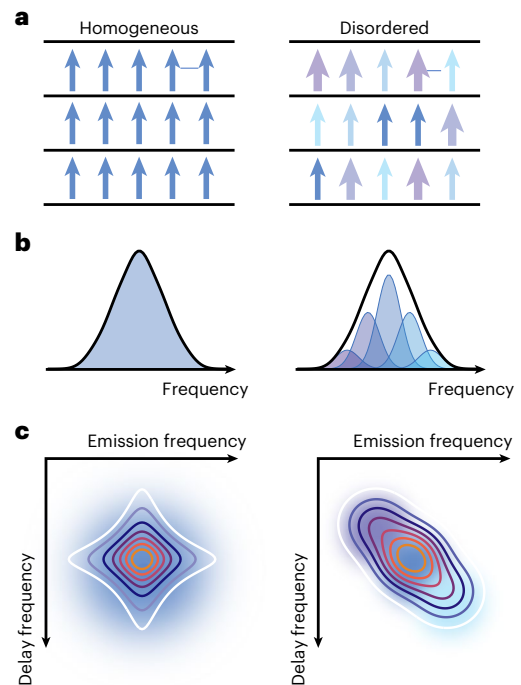


Fig. 3 | Disorder in schematic one- and two-dimensional spectra. **a**, A cartoon of homogeneous and disordered Josephson tunnelling in a layered superconductor. **b**, Homogeneous and disordered Josephson plasma resonance in one-dimensional spectra, which exhibit ambiguous lineshapes (black curves) in the presence of comparable levels of intrinsic and disorder broadening. **c**, Homogeneous and disordered Josephson plasma resonance in 2D Josephson echo spectra, in which disorder is evident through asymmetry of the Josephson echo peak.

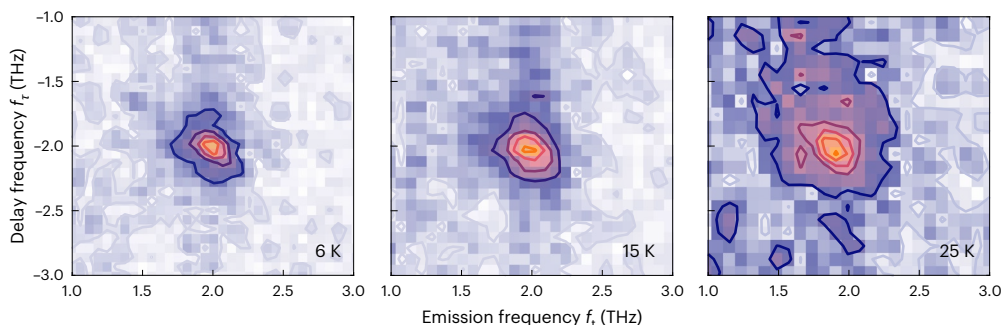


Fig. 4 | Two-dimensional Josephson echo spectra of $\text{La}_{1.83}\text{Sr}_{0.17}\text{CuO}_4$ for increasing temperatures. Two-dimensional spectra in the $(f_e, f_i) = (f_p, -f_p)$ quadrant with equal-value contours plotted on top of the raw data. At the lowest

temperature of 6 K, ‘almond’ asymmetry of the peak is clearly observed that indicates the presence of disorder. At higher temperatures, the peak lineshape becomes increasingly symmetric due to a lesser relative importance of disorder.

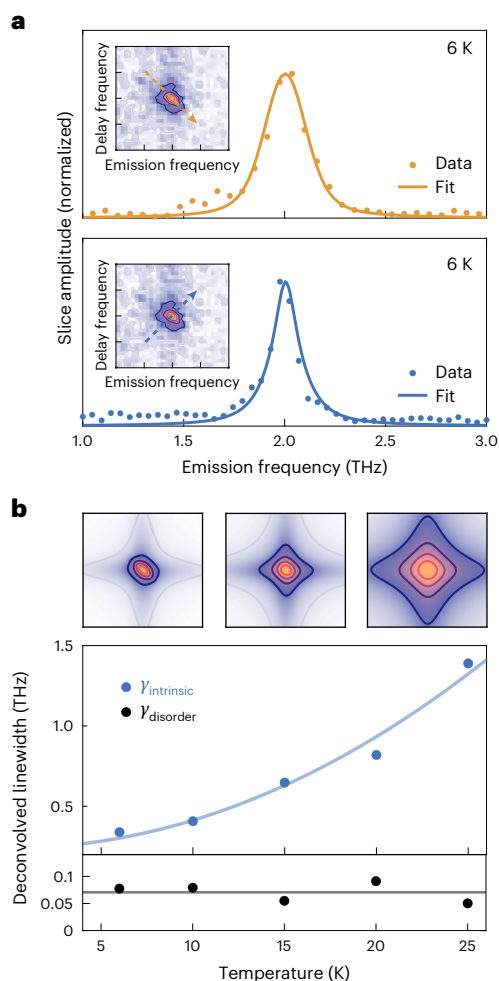


Fig. 5 | Fitting the Josephson echo peak lineshape to extract intrinsic and disorder linewidths. **a**, Slices of the Josephson echo peak at 6 K along the ‘diagonal’ (orange) and ‘anti-diagonal’ (blue) directions shown (inset). The

lineshapes of both slices are broadened by intrinsic damping and disorder, and fits of the two lineshapes are thus performed simultaneously to extract γ_{disorder} and $\gamma_{\text{intrinsic}}$. **b**, The temperature dependence of γ_{disorder} and $\gamma_{\text{intrinsic}}$, in which disorder of the Josephson plasma resonance remains roughly constant while its intrinsic damping increases rapidly with temperature. The lines are guides to the eye, and the 2D spectra shown above are simulated with the fitted parameters at 6 K, 15 K and 25 K from left to right, respectively.

of increasing temperature. First, the intrinsic linewidth $\gamma_{\text{intrinsic}}$ increases rapidly with temperature owing to thermally activated quasiparticle excitations or perhaps even topological defects⁴⁵. More surprising is the behaviour of the disorder linewidth γ_{disorder} , which remains roughly constant up to a temperature of 25 K $\approx 0.7T_c$. Above this temperature, the Josephson plasma resonance becomes lifetime limited and the disorder becomes unmeasurable.

One may expect the disorder to increase with temperature as the coherence length (reflecting the spatial extent of the Cooper wavefunction⁴⁶) shrinks⁴⁷. The independence of γ_{disorder} with respect to temperature thus raises the question of whether the disorder linewidth already reflects the full extent of the underlying electronic disorder. We compare in Fig. 6 the measured distribution of plasma frequencies (of standard deviation γ_{disorder}) with the previously measured superconducting gap distribution in LSCO⁵. The large difference between the two distribution widths indicates, however, that in-plane disorder of the superconducting order parameter is not directly reflected in disorder of the out-of-plane transport.

We may intuitively understand the difference between the in-plane disorder of the superconducting order parameter to resultant disorder of the out-of-plane tunnelling resonance by considering its broadening effect on the linear optical response, from which the nonlinear optical response partially descends. Namely, assuming that the superfluid density directly inherits identical disorder from the underlying gap fluctuations (due to the short coherence length⁴⁸ in LSCO⁴⁹), one expects a disorder broadening of the linear optical response suppressed by the plasma frequency anisotropy $(\omega_p/\omega_{ab})^2 \ll 1$.

Our preliminary theoretical analysis of γ_{disorder} , which will be presented elsewhere, indicates that the many-body nature of Josephson plasmons introduces additional physics beyond the well-known interpretation of molecular photon echoes or spin echoes. Most notably, the momentum dependence that arises in extended systems prevents complete rephasing of collective excitations, resulting in an additional ‘homogeneous-like’ background. We emphasize however, that the primary rephased component still exhibits the elongated peak lineshape characteristic of disorder echoes and observed in our measurements.

Recent advances in tunnelling methods^{8–11} will also provide new data to corroborate our conclusions and to systematically connect these two methods. We note, however, that local probes are effective only at the lowest base temperatures, whereas the optical method demonstrated here is already applied up to $0.7T_c$ in this work. Nonlinear multidimensional responses are even observed immediately above T_c , although fitting of their corresponding Josephson echo signal is currently prevented by small signal amplitudes and signal-to-noise ratio. Suitable technical improvements will enable nonlinear probing of the partially coherent normal state and may provide precious new information on the nature of the pseudogap phase. We also note how new and frequency-agile terahertz

and uniquely enables us to follow disorder in the superconducting transport even at temperatures approaching the phase transition. Extracted values of γ_{disorder} and $\gamma_{\text{intrinsic}}$ are shown in Fig. 5b as a function

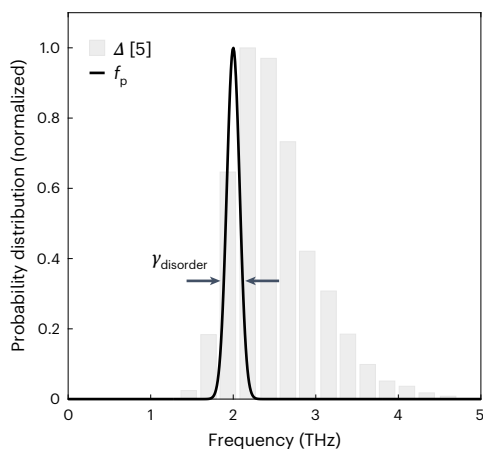


Fig. 6 | Comparison of disorder in the superconducting gap and in the superconducting transport. A probability distribution for the Josephson plasma frequencies f_p (solid line) is compared with that of the superconducting gap Δ (shaded bars) measured using scanning tunnelling microscopy⁵, measured at 6 K and 4.2 K, respectively. The standard deviation of the plasma frequency distribution $\gamma_{\text{disorder}} = 78$ GHz is far smaller than the standard deviation of the superconducting gap $\gamma_{\Delta} = 2.8$ THz.

sources, which are becoming available due to improvements in laser instrumentation⁵⁰, will enable systematic measurements throughout the phase diagram of a single compound and across many families of cuprates, where frequencies of the plasma resonance vary between 100 GHz and 15 THz (ref. 12).

In summary, we have made use of 2D terahertz spectroscopy to quantify the role of disorder in the interlayer tunnelling and, thereby, in the superconducting condensate. By measuring the terahertz Josephson echo, we observe an interlayer tunnelling response that is largely immune to the underlying electronic disorder, which remains true even as temperature approaches the phase transition. This demonstration of terahertz echoes²⁷ from a collective excitation provides us with a method to study inhomogeneities in a vast range of quantum materials, ranging from incipient ferroelectrics⁵¹ to spin liquids⁵². Furthermore, the inherent ultrafast nature of this method makes it applicable to multidimensional probes of light-induced non-equilibrium phenomena^{53,54} to understand the role of disorder in transient states and their formation mechanisms.

Online content

Any methods, additional references, Nature Portfolio reporting summaries, source data, extended data, supplementary information, acknowledgements, peer review information; details of author contributions and competing interests; and statements of data and code availability are available at <https://doi.org/10.1038/s41567-024-02643-5>.

References

- Singer, P. M., Hunt, A. W. & Imai, T. ⁶³Cu NQR evidence for spatial variation of hole concentration in $\text{La}_{2-x}\text{Sr}_x\text{CuO}_4$. *Phys. Rev. Lett.* **88**, 047602 (2002).
- Bozin, E. S., Kwei, G. H., Takagi, H. & Billinge, S. J. L. Neutron diffraction evidence of microscopic charge inhomogeneities in the CuO_2 plane of superconducting $\text{La}_{2-x}\text{Sr}_x\text{CuO}_4$ ($0 \leq x \leq 0.30$). *Phys. Rev. Lett.* **84**, 5856 (2000).
- Yazdani, A., da Silva Neto, E. H. & Aynajian, P. Spectroscopic imaging of strongly correlated electronic states. *Annu. Rev. Condens. Matter Phys.* **7**, 11–13 (2016).
- Pan, S. H. et al. Microscopic electronic inhomogeneity in the high- T_c superconductor $\text{Bi}_2\text{Sr}_2\text{CaCu}_2\text{O}_{8+x}$. *Nature* **413**, 282–285 (2001).
- Kato, T., Okitsu, S. & Sakata, H. Inhomogeneous electronic states of $\text{La}_{2-x}\text{Sr}_x\text{CuO}_4$ probed by scanning tunneling spectroscopy. *Phys. Rev. B* **72**, 144518 (2005).
- McElroy, K. et al. Atomic-scale sources and mechanism of nanoscale electronic disorder in $\text{Bi}_2\text{Sr}_2\text{CaCu}_2\text{O}_{8+\delta}$. *Science* **309**, 1048–1052 (2005).
- Proslir, T. et al. Probing the superconducting condensate on a nanometer scale. *EPL* **73**, 962–968 (2006).
- Hamidian, M. H. et al. Detection of a Cooper-pair density wave in $\text{Bi}_2\text{Sr}_2\text{CaCu}_2\text{O}_{8+x}$. *Nature* **532**, 343–347 (2016).
- Cho, D., Bastiaans, K. M., Chatzopoulos, D., Gu, G. D. & Allan, M. P. A strongly inhomogeneous superfluid in an iron-based superconductor. *Nature* **571**, 541–545 (2019).
- Liu, X., Chong, Y. X., Sharma, R. & Davis, J. C. Atomic-scale visualization of electronic fluid flow. *Nat. Mater.* **20**, 1480–1484 (2021).
- Liu, X., Chong, Y. X., Sharma, R. & Davis, J. C. Discovery of a Cooper-pair density wave state in a transition-metal dichalcogenide. *Science* **372**, 1447–1452 (2021).
- Laplace, Y. & Cavalleri, A. Josephson plasmonics in layered superconductors. *Adv. Phys. X* **1**, 387–411 (2016).
- Gabriele, F., Castellani, C. & Benfatto, L. Generalized plasma waves in layered superconductors: a unified approach. *Phys. Rev. Res.* **4**, 023112 (2022).
- Tamasaku, K., Nakamura, Y. & Uchida, S. Charge dynamics across the CuO_2 planes in $\text{La}_{2-x}\text{Sr}_x\text{CuO}_4$. *Phys. Rev. Lett.* **69**, 1455 (1992).
- Basov, D. N. & Timusk, T. Electrodynamics of high- T_c superconductors. *Rev. Mod. Phys.* **77**, 721 (2005).
- Van der Marel, D. & Tsvetkov, A. Transverse optical plasmons in layered superconductors. *Czech. J. Phys.* **46**, 3165–3168 (1996).
- Dressel, M. & Grüner, G. *Electrodynamics of Solids* (Cambridge Univ. Press, 2010).
- Dordevic, S. V., Komiya, S., Ando, Y. & Basov, D. N. Josephson plasmon and inhomogeneous superconducting state in $\text{La}_{2-x}\text{Sr}_x\text{CuO}_4$. *Phys. Rev. Lett.* **91**, 167401 (2003).
- Mukamel, S. *Principles of Nonlinear Optical Spectroscopy* (Oxford Univ. Press, 1995).
- Turner, D. B. & Nelson, K. A. Coherent measurements of high-order electronic correlations in quantum wells. *Nature* **466**, 1089–1092 (2010).
- Mukamel, S., Tanimura, Y. & Hamm, P. Coherent multidimensional optical spectroscopy. *Acc. Chem. Res.* **42**, 1207–1209 (2009).
- Reimann, K., Woerner, M. & Elsaesser, T. Two-dimensional terahertz spectroscopy of condensed-phase molecular systems. *J. Chem. Phys.* **154**, 120901 (2021).
- Savolainen, J., Ahmed, S. & Hamm, P. Two-dimensional Raman-terahertz spectroscopy of water. *Proc. Natl Acad. Sci. USA* **110**, 20402–20407 (2013).
- Maag, T. et al. Coherent cyclotron motion beyond Kohn's theorem. *Nat. Phys.* **12**, 119–123 (2016).
- Somma, C., Folpini, G., Reimann, K., Woerner, M. & Elsaesser, T. Two-phonon quantum coherences in indium antimonide studied by nonlinear two-dimensional terahertz spectroscopy. *Phys. Rev. Lett.* **116**, 177401 (2016).
- Grechko, M. et al. Coupling between intra- and intermolecular motions in liquid water revealed by two-dimensional terahertz-infrared-visible spectroscopy. *Nat. Commun.* **9**, 885 (2018).
- Lu, J. et al. Nonlinear two-dimensional terahertz photon echo and rotational spectroscopy in the gas phase. *Proc. Natl Acad. Sci. USA* **113**, 11800–11805 (2016).
- Johnson, C. L., Knighton, B. E. & Johnson, J. A. Distinguishing nonlinear terahertz excitation pathways with two-dimensional spectroscopy. *Phys. Rev. Lett.* **122**, 073901 (2019).

29. Mahmood, F., Chaudhuri, D., Gopalkrishnan, S., Nandkishore, R. & Armitage, N. P. Observation of a marginal Fermi glass. *Nat. Phys.* **17**, 627–631 (2021).
30. Pal, S. et al. Origin of terahertz soft-mode nonlinearities in ferroelectric perovskites. *Phys. Rev. X* **11**, 021023 (2021).
31. Lin, H. W., Mead, G. & Blake, G. A. Mapping LiNbO₃ phonon-polariton nonlinearities with 2D THz-THz-Raman spectroscopy. *Phys. Rev. Lett.* **129**, 207401 (2022).
32. Houver, S., Huber, L., Savoini, M., Abreu, E. & Johnson, S. L. 2D THz spectroscopic investigation of ballistic conduction-band electron dynamics in InSb. *Opt. Expr.* **27**, 10854–10865 (2019).
33. Blank, T. G. H. et al. Two-dimensional terahertz spectroscopy of nonlinear phononics in the topological insulator MnBi₂Te₄. *Phys. Rev. Lett.* **131**, 026902 (2023).
34. Zhang, Z. et al. Terahertz field-induced nonlinear coupling of two magnon modes in an antiferromagnet. *Nat. Phys.* <https://doi.org/10.1038/s41567-024-02386-3> (2024).
35. Zhang, Z. et al. Terahertz-field-driven magnon upconversion in an antiferromagnet. *Nat. Phys.* <https://doi.org/10.1038/s41567-023-02350-7> (2024).
36. Luo, L. et al. Quantum coherence tomography of light-controlled superconductivity. *Nat. Phys.* **19**, 201–209 (2023).
37. Mootz, M., Luo, L., Wang, J. & Perakis, I. E. Visualization and quantum control of light-accelerated condensates by terahertz multi-dimensional coherent spectroscopy. *Commun. Phys.* **5**, 1–10 (2022).
38. Kim, M.-J. et al. Tracing the dynamics of superconducting order via transient third harmonic generation. *Sci. Adv.* **10**, eadi7598 (2023).
39. Honold, A., Schultheis, L., Kuhl, J. & Tu, C. W. Reflected degenerate four-wave mixing on GaAs single quantum wells. *Appl. Phys. Lett.* **52**, 2105–2107 (1988).
40. Rajasekaran, S. et al. Parametric amplification of a superconducting plasma wave. *Nat. Phys.* **12**, 1012–1016 (2016).
41. Zhang, S. et al. Revealing the frequency-dependent oscillations in nonlinear terahertz response induced by Josephson current. *Natl Sci. Rev.* **10**, nwad163 (2023).
42. Siemens, M. E., Moody, G., Li, H., Bristow, A. D. & Cundiff, S. T. Resonance lineshapes in two-dimensional Fourier transform spectroscopy. *Opt. Expr.* **18**, 17699–17708 (2010).
43. Bristow, A. D., Zhang, T., Siemens, M. E., Cundiff, S. T. & Mirin, R. P. Separating homogeneous and inhomogeneous line widths of heavy- and light-hole excitons in weakly disordered semiconductor quantum wells. *J. Phys. Chem. B* **115**, 5365–5371 (2011).
44. Liu, A., Cundiff, S. T., Almeida, D. B. & Ulbricht, R. Spectral broadening and ultrafast dynamics of a nitrogen-vacancy center ensemble in diamond. *Mater. Quantum Technol.* **1**, 025002 (2021).
45. Koshelev, A. E. & Bulaevskii, L. N. Fluctuation broadening of the plasma resonance line in the vortex liquid state of layered superconductors. *Phys. Rev. B* **60**, R3743 (1999).
46. Tinkham, M. *Introduction to Superconductivity* (Dover Publications, 2004).
47. Ginsberg, D. M. Calculation of the temperature dependence of the electromagnetic coherence length in superconductors. *Phys. Rev. B* **7**, 146 (1973).
48. Deutscher, G. The role of the short coherence length in unconventional superconductors. *Condens. Matter* **5**, 77 (2020).
49. Wesche, R. *Physical Properties of High-Temperature Superconductors* (Wiley-VCH, 2015).
50. Liu, B., Bromberger, H., Cartella, A., Först, M. & Cavalleri, A. Generation of narrowband, high-intensity, carrier-envelope phase-stable pulses tunable between 4 and 18 THz. *Opt. Lett.* **42**, 129–131 (2017).
51. Müller, K. A. & Burkhard, H. SrTiO₃: an intrinsic quantum paraelectric below 4 K. *Phys. Rev. B* **19**, 3593 (1979).
52. Wan, Y. & Armitage, N. P. Resolving continua of fractional excitations by spin echo in THz 2D coherent spectroscopy. *Phys. Rev. Lett.* **122**, 257401 (2019).
53. Bao, C., Tao, P., Sun, D. & Zhou, S. Light-induced emergent phenomena in 2D materials and topological materials. *Nat. Rev. Phys.* **4**, 33–48 (2022).
54. Disa, A. S., Nova, T. F. & Cavalleri, A. Engineering crystal structures with light. *Nat. Phys.* **17**, 1087–1092 (2021).

Publisher's note Springer Nature remains neutral with regard to jurisdictional claims in published maps and institutional affiliations.

Open Access This article is licensed under a Creative Commons Attribution 4.0 International License, which permits use, sharing, adaptation, distribution and reproduction in any medium or format, as long as you give appropriate credit to the original author(s) and the source, provide a link to the Creative Commons licence, and indicate if changes were made. The images or other third party material in this article are included in the article's Creative Commons licence, unless indicated otherwise in a credit line to the material. If material is not included in the article's Creative Commons licence and your intended use is not permitted by statutory regulation or exceeds the permitted use, you will need to obtain permission directly from the copyright holder. To view a copy of this licence, visit <http://creativecommons.org/licenses/by/4.0/>.

© The Author(s) 2024

Methods

The sample used in our experiment was a single crystal of $\text{La}_{1.83}\text{Sr}_{0.17}\text{CuO}_4$, grown using the travelling-solvent floating-zone method. The crystal was cut and mechanically polished using diamond lapping film along an *ac*-oriented surface ~ 4 mm in size.

To perform 2D terahertz spectroscopy, two intense terahertz pulses were generated by optical rectification of 100 fs, 1,300 nm pulses in two OH1 (2-{3-(4-hydroxystyryl)-5,5-dimethylcyclohex-2-enylidene} malononitrile) organic crystals. The two terahertz pulses are then focused in a non-collinear geometry onto the sample with a parabolic mirror of focal length 76.2 mm (ref. 55), resulting in peak electric fields of -25 kV cm^{-1} and -10 kV cm^{-1} at the sample surface (Supplementary Section 1) that together are comparable to the threshold electric field for reaching a nonlinear regime $E_{\text{thresh}} = (hf_p)/2ed \approx 40 \text{ kV cm}^{-1}$ (ref. 40), where h is Planck's constant, $2e$ is the Cooper pair charge and d is the interlayer spacing. The emitted nonlinear electric field was then detected by conventional electro-optic sampling using 100 fs, 800 nm pulses in a ZnTe crystal. A differential chopping scheme, in which E_A and E_B were modulated at 500 Hz and 333 Hz, respectively, was used to isolate the nonlinear electric field from the excitation fields.

Data availability

Source data are provided with this paper. Any other supporting data are available from the corresponding authors upon reasonable request.

References

55. Liu, A. Off-axis imaging with off-axis parabolic mirrors. *Appl. Opt.* **62**, 8574–8576 (2023).

Acknowledgements

A.L. and M.H.M. gratefully acknowledge funding from the Alexander von Humboldt Foundation. E.D. acknowledges support from the SNSF project no. 200021_212899. E.D., and P.E.D. acknowledge support from

the Army Research Office under grant no. W911NF-21-1-0184. The work at BNL was supported by the US Department of Energy (DOE), Office of Basic Energy Sciences (BES) under contract no. DOE-SC0012704.

Author contributions

A.L. and A.C. conceived this project. The 2D terahertz spectroscopy experiments were carried out by A.L. and D.P. The resultant data were analysed by A.L., and M.H.M., and E.D. developed a theoretical model for disorder broadening of plasmons together with A.G.S. and P.E.D. A.D. and M.F. contributed to the discussion and interpretation of results. P.L., Q.L. and G.D.G. prepared and provided the single-crystal LSCO samples. The paper was written by A.L. and A.C. with contributions from all other authors.

Funding

Open access funding provided by Max Planck Society.

Competing interests

The authors declare no competing interests.

Additional information

Supplementary information The online version contains supplementary material available at <https://doi.org/10.1038/s41567-024-02643-5>.

Correspondence and requests for materials should be addressed to A. Liu or A. Cavalleri.

Peer review information *Nature Physics* thanks the anonymous reviewers for their contribution to the peer review of this work.

Reprints and permissions information is available at www.nature.com/reprints.